PHYSICAL REVIEW B **86**, 155443 (2012)

Dynamics of Ti, N, and TiN$_x$ (x = 1–3) admolecule transport on TiN(001) surfaces

D. G. Sangiovanni,[1,*] D. Edström,[1] L. Hultman,[1] V. Chirita,[1] I. Petrov,[1,2] and J. E. Greene[1,2]
[1]*Department of Physics, Chemistry and Biology (IFM), Linköping University, SE-58183 Linköping, Sweden*
[2]*Frederick Seitz Materials Research Laboratory and the Materials Science Department, University of Illinois at Urbana-Champaign, Urbana, Illinois 61801, USA*

(Received 29 May 2012; revised manuscript received 4 September 2012; published 22 October 2012)

We use classical molecular dynamics and the modified embedded atom method formalism to investigate the dynamics of atomic-scale transport on a low-index model compound surface, TiN(001). Our simulations, totaling 0.25 μs for each case study, follow the pathways and migration kinetics of Ti and N adatoms, as well as TiN$_x$ complexes with x = 1–3, which are known to contribute to the growth of TiN thin films by reactive deposition from Ti, N$_2$, and N precursors. The simulations are carried out at 1000 K, within the optimal range for TiN(001) epitaxial growth. We find Ti adatoms to be the highest-mobility species on TiN(001), with the primary migration path involving jumps of one nearest-neighbor distance d_{NN} between adjacent fourfold hollow sites along in-plane $\langle 100\rangle$ channels. Long jumps, $2d_{\mathrm{NN}}$, are also observed, but at much lower frequency. N adatoms, which exhibit significantly lower migration rates than Ti, diffuse along in-plane $\langle 110\rangle$ directions and, when they intersect other N atoms, associatively form N$_2$ molecules, which desorb at kinetic rates. As expected, TiN and TiN$_3$ complexes migrate at even lower rates with complex diffusion pathways involving rotations, translations, and rototranslations. TiN$_2$ trimers, however, are shown to have surprisingly high diffusion rates, above that of N adatoms and almost half that of Ti adatoms. TiN$_3$ motion is dominated by in-place rotation with negligible diffusion.

DOI: 10.1103/PhysRevB.86.155443 PACS number(s): 83.10.Rs, 68.43.Jk, 81.10.Aj, 71.15.Mb

I. INTRODUCTION

Thin-film growth is a complex process controlled by the interplay of thermodynamic driving forces and kinetically controlled atomistic responses. Fundamental understanding of processes governing nanostructural and surface morphological evolution during thin-film growth requires detailed information regarding the dynamics of atomic-scale transport on surfaces.

Most surface dynamics studies for determining rate-limiting mechanisms, step energies, and mass transport parameters, assume surface isotropy and isotropic processes.[1] However, this is not always the case, especially for compound surfaces, including the low-index planes of commercially important materials systems such as GaN, GaAs, and Al$_2$O$_3$, known to be highly anisotropic.[1–3] In addition, state-of-the-art atomic-scale experimental techniques, including scanning tunneling microscopy (STM)[4–6] and low-energy electron microscopy (LEEM),[7–9] cannot resolve picosecond time-scale surface dynamics; hence, complementary computational studies are required. For small systems, first-principles calculations have been used to determine the energetics of cation adsorption and diffusion on static transition-metal (TM) nitride surfaces.[10–12] However, system sizes required for dynamics studies are prohibitively large for computational methods such as density functional theory (DFT). This renders classical molecular dynamics (MD) as the primary fully deterministic computational technique available to resolve the dynamics of atomic-scale processes on compound surfaces.

Here, we report the initial results of studies of atomistic transport processes leading to epitaxial growth on TiN(001). Titanium nitride, one of the first hard-coating materials,[13–15] serves as a model for NaCl-structure TM nitride compounds and alloys presently used in a wide variety of applications based upon their unique properties: high hardness,[13,16] excellent scratch and abrasion resistance,[17] relatively low coefficient of friction,[18] high-temperature oxidation resistance,[19–21] metallic to semiconducting conductivity,[22] optical absorption, which can be tuned across the visible spectrum,[22] and superconductivity.[23,24] Nanocomposites[25] and superlattices[26] based upon TM nitride constituents have been shown to be superhard (hardness $\geqslant$40 GPa).

Among TM nitrides, TiN is the most extensively investigated experimentally using, for example, *in situ* variable-temperature scanning tunneling microscopy (VT-STM) to probe nucleation,[10,27] growth,[5,6,28,29] and microstructural and surface morphological evolution.[30,31] VT-STM nucleation studies, combined with DFT calculations,[10,11] have shown that the primary diffusing species during the epitaxial growth of TiN(001) are Ti, N, and TiN$_x$ complexes (x = 1–3), where the dominant N-containing admolecule depends upon the incident N/Ti flux ratio.

As a first step in the investigation of atomic-scale kinetic transport processes on TiN(001), we use classical MD to determine activation energies and surface pathways for the diffusion of Ti and N adatoms as well as TiN$_x$ complexes, with x = 1–3. TiN$_4$ has been shown to be unstable to dissociation of TiN$_2$ + N$_2$, where N$_2$ desorbs at kinetic rates during film growth.[11] The time resolution of our MD runs allows for accurate calculation of migration kinetics; the results show that Ti adatoms have significantly higher diffusion rates than N adatoms on TiN(001). For TiN$_x$ complexes, we find, consistent with the lower mobility of N adatoms and the expected increase in diffusion barriers for larger clusters, a significant decrease in TiN$_x$ diffusion rates for TiN$_3$ vs TiN admolecules. However, TiN$_2$ trimers exhibit surprisingly high mobilities, comparable to those of Ti adatoms.

The primary diffusion pathways for N and Ti adatoms are single jumps along energetically favored [110] directions for N and [100] and [010] channels for Ti, exhibiting strong TiN(001) diffusional anisotropy. Long jumps are also observed for Ti, but they are rare (∼5%). For TiN_x complexes, migration pathways involve considerably more complex motions: rotations, concerted translations, and rototranslations.

II. METHODOLOGY

We perform classical MD simulations using the open-source code Large-Scale Atomic/Molecular Massively Parallel Simulator (LAMMPS),[32] distributed by Sandia National Laboratories. Atomic interactions are described by implementing the protocol for the second nearest-neighbor (2NN) modified embedded atom method (MEAM).[33] Within the MEAM formalism, the total energy of a system is expressed as

$$E = \sum_i \left[F_i(\bar{\rho}_i) + \frac{1}{2} \sum_{j(\neq i)} S_{ij}\phi_{ij}(R_{ij}) \right], \tag{1}$$

where F_i is the energy to embed atom i within the electron density $\bar{\rho}_i$, $\phi_{ij}(R_{ij})$ is the pair interaction of atoms i and j as a function of separation distance R_{ij}, and S_{ij} is a screening function.[33]

Recently, MEAM parameters have been published for TiN.[34] MEAM parameters for compounds are typically fit to both elemental constituent and compound properties such as cohesive energy, enthalpy of formation, lattice parameter, and bulk moduli, and then optimized to reproduce fundamental structural, elastic, and surface properties. While this approach allows simulation of bulk phenomena, MEAM parameters used in MD simulations of thin-film growth require additional testing to accurately represent essential surface properties such as surface diffusion and Ehrlich step-edge barriers for adatoms and small clusters.

In preliminary tests with the original MEAM parameters for TiN,[34] we find N adatoms to have a significantly lower surface diffusion barrier ($E_s = 0.8$ eV) than Ti adatoms (1.0 eV) on TiN(001), while DFT calculations yield $E_s = 0.43$ eV for Ti adatoms and 0.95 eV for N adatoms. In addition, the results for the migration of TiN dimers on TiN(001) appear unphysical. Within a few MD steps, N atoms move atop Ti atoms such that the dimer axis is normal to the surface, as in the polar [111] direction, rather than in-plane as expected for the nonpolar (001) surface.

To address these issues, we modify six N-N interaction and three Ti-N screening parameters, for a total of 39 MEAM parameters, and optimize them using reference values obtained from DFT calculations carried out within the Vienna *Ab initio* Simulation Package (VASP) code[35] implemented in the Perdew-Wang generalized gradient approximation (GGA).[36] Electron-ion interactions are described with projector-augmented-wave potentials (PAW).[37] Total energies are evaluated to an accuracy of 10^{-5} eV/atom with a large plane-wave basis-set energy cutoff of 500 eV; the Brillouin zone is sampled with 15 × 15 × 1 k-point grids. Adatom diffusion barriers are calculated by DFT on relaxed TiN(001) slabs consisting of five atomic layers and six vacuum layers, for a total of 80 atoms. We obtain surface diffusion energy barriers of 0.43 eV for Ti and 0.95 eV for N, in excellent agreement with previous DFT results.[11]

TABLE I. Original and modified MEAM parameters used to describe N-N and Ti-N interactions.

MEAM parameters	Original[34]	Present
N-N		
A	1.80	1.73
$\beta^{(0)}$	2.75	2.74
$\beta^{(2)}$	4.0	4.3
$t^{(1)}$	0.05	0.10
$t^{(2)}$	1.0	1.2
$t^{(3)}$	0.0	0.5
Ti-N		
α	5.092	4.885
$C_{\min}$(Ti,Ti,N)	0.16	0.01
$C_{\max}$(N,N,Ti)	2.80	2.93

The optimized MEAM parameters used in this study are listed in Table I; all other parameters are identical to the original ones.[34] As shown in Table II, our modified parameters yield TiN bulk properties and low-index surface formation energies, which are in excellent agreement with those obtained using the original MEAM parameters,[34] as well as with experimental[5,29,38–42] and DFT[11,43–45] results. The trend in diffusion barriers obtained using our parameterization, $E_s = 0.8$ eV for Ti and 1.1 eV for N adatoms, is in qualitative agreement with DFT results, which give lower barriers for Ti diffusion, and significantly closer to the experimentally determined range (1.1–1.4 eV, depending upon N_2 partial pressure),[27] as shown in Table III. TiN(001) surface relaxation, in which N terrace atoms move outward 0.12 Å, on average, and Ti atoms move inward 0.11 Å, is also in agreement with DFT calculations.[11,44] Moreover, within the current implementation, TiN dimers diffuse as expected on TiN(001), with the Ti-N bond axis parallel to the surface, and from static calculations, we determine Ehrlich barriers of ∼0.8 eV for Ti (Fig. 1) and ∼0.0–0.1 eV for N, consistent with a global experimental value of ∼0.5 eV on TiN(001).[6] We obtain adatom formation energies of ∼1.0 eV for Ti and ∼2.0 eV for N, consistent with the experimental range 1.2 to 2.0 eV.[4,27]

MD calculations are performed in the microcanonical ensemble (NVE),[46] using a time step of 1 fs and a thermostat to maintain temperature constant at 1000 K, which is within the optimum range for growth of epitaxial TiN(001) layers.[16,47] The TiN(001) simulation slab consists of six layers of 18 × 18 atoms, as illustrated in Fig. 2(a). All atoms in the simulation cell are allowed to relax, and the temperature in the system is maintained constant via velocity rescaling. To simulate free surfaces, the periodicity in the [001] direction is removed, and the surface allowed to relax [Fig. 2(b)]; the lattice constant increases ∼0.5% due to the thermal expansion at 1000 K. Single Ti and N adatoms and TiN_x complexes are initially placed above the substrate at a distance of 2.2 Å, slightly higher than the first nearest-neighbor Ti-N bulk distance, $d_{\text{NN}} = 2.12$ Å. For each case study, we use statistically independent MD runs of 10 ns to monitor diffusion for total simulation times of 0.25 μs. The results are stored in video files with 75-fs resolution. Migration pathways are followed, and total migration distances reported in units of d_{NN}

TABLE II. Bulk and surface TiN properties calculated using the present MEAM parameter set compared with results calculated with the original MEAM parameters[34] as well as *ab initio* and experimental results. E_c = TiN cohesive energy; a = TiN lattice constant; B = TiN bulk modulus; C_{11}, C_{12}, and C_{44} = TiN elastic constants; $E_{\text{step-edge}}$ (001) = TiN(001) step-edge energy; E_{surf} unrel(rel) = formation energy of unrelaxed (relaxed) TiN surfaces; Δ(N$_1$-Ti$_1$) (001) = average z spacing between N and Ti atoms in the relaxed TiN(001) surface layer; Δ(N$_1$-Ti$_2$) (001) = z coordinate variation (relative to d_{NN}) between upper-layer N atoms and second-layer Ti atoms in relaxed TiN(001); and Δ(Ti$_1$-N$_2$) (001) = z coordinate variation (relative to d_{NN}) between upper-layer Ti atoms and second-layer N atoms in relaxed TiN(001).

Properties	MEAM present parameters	MEAM[34] original parameters	*Ab initio* calculations	Experimental results
E_c (eV/atom)	6.615	6.615	7.120,[a] 7.165[11]	
a (Å)	4.242	4.242	4.255,[a] 4.254,[43] 4.175–4.260[44]	4.240,[38] 4.240[39]
B (GPa)	295	320	295,[a] 290,[43] 265–319[44]	346,[39] 318,[40] 288[41]
C_{11} (GPa)	671	659	640,[43] 561–704[44]	626,[39] 625[40]
C_{12} (GPa)	107	150	115,[43] 116–125[44]	206,[39] 165[40]
C_{44} (GPa)	170	183	159,[43] 156–168[44]	156,[39] 163[40]
$E_{\text{step-edge}}$ (001) (eV/Å)	0.23	0.22[b]	0.26,[a] 0.24[45]	0.23,[5] 0.25[29]
E_{surf} (001) unrel (J/m^2)	1.83	1.78	1.57,[a] 1.60,[11] 1.53–1.76[44]	
E_{surf} (001) rel (J/m^2)	1.45	1.30	1.24,[a] 1.30,[11] 1.06–1.30[44]	1.1[42]
E_{surf} (110) unrel (J/m^2)	2.98	2.89	2.87–3.14[44]	
E_{surf} (110) rel (J/m^2)	2.56	2.46	2.59–2.86[44]	
E_{surf} (001)/E_{surf} (110)	0.57	0.53	0.41–0.45[44]	0.7[42]
E_{surf} (111) unrel (J/m^2)	3.93	3.92	4.97,[11] 5.08–5.45[44]	
E_{surf} (111) rel (J/m^2)	3.66	3.65	3.45,[11] 4.59–4.95[44]	
Δ(N$_1$-Ti$_1$) (001) (Å)	0.234	0.256	0.174,[a] 0.18,[11] 0.179[44]	
Δ(N$_1$-Ti$_2$) (001) (%)	5.8	7.7	3.2,[a] 2.1[44]	
Δ(Ti$_1$-N$_2$) (001) (%)	−5.3	−5.0	−5.9,[a] −6.3[44]	

[a] Present results.

[b] Present results using parameters of Ref. 34.

by tracing N, Ti, and TiN$_x$ geometric center (GC) trajectories. For single adatoms and TiN$_2$ trimers, GC corresponds to the center of mass. Similar to classical MD studies investigating thin-film growth on Pt(111) surfaces,[48,49] we calculate both total distances traveled along the trajectories as well as average net distances between initial and final GC positions.

Surface diffusion coefficients D are obtained for each adspecies based upon the two-dimensional Einstein relation

$$D = \lim_{t\to\infty} \frac{\langle[\vec{r}(t)-\vec{r}(0)]^2\rangle}{4t}, \tag{2}$$

where $\vec{r}(t)$ is the adspecies GC x,y position at time t, and $\langle[\vec{r}(t)-\vec{r}(0)]^2\rangle$ is the mean-square displacement. Using our calculated diffusion activation energies E_s and surface diffusion coefficients D, we determine the exponential prefactors D_0 from the Arrhenius equation:

$$D = D_0 \exp\left(-\frac{E_s}{k_B T}\right). \tag{3}$$

III. RESULTS

The energetically favored positions on an empty TiN(001) terrace, away from step edges, are fourfold hollow sites, for both N and Ti adatoms, surrounded by two N and two Ti terrace atoms. We obtain, based upon static calculations, adsorption energies E_{ad} of −1.8 eV for N and −5.1 eV for Ti. Thus, fourfold hollow terrace sites are chosen as starting positions

TABLE III. Calculated surface diffusion barriers E_s for N and Ti adatoms and TiN$_x$ (x = 1–3) admolecules on TiN(001) using the present MEAM parameter set compared with results obtained using the original TiN parameterization[34] as well as *ab initio* and experimental results.

Diffusing species	Diffusion barriers E_s (eV) MEAM present parameters	MEAM[b] original parameters	Experimental[27] results	DFT calculations
Ti adatom	0.8	1.0		0.35,[11] 0.43[c]
N adatom	1.1	0.8		0.95,[11] 0.95[c]
TiN dimer	>1.1[a]			⩾0.88[11]
TiN$_2$ trimer	0.8–1.1[a]			
TiN$_3$ tetramer	≫1.1[a]			
TiN$_x$			1.1–1.4	

[a] Estimated from the comparison of TiN$_x$ mobilities with adatom mobilities.

[b] Obtained with the parameterization reported in Ref. 34.

[c] Present results.

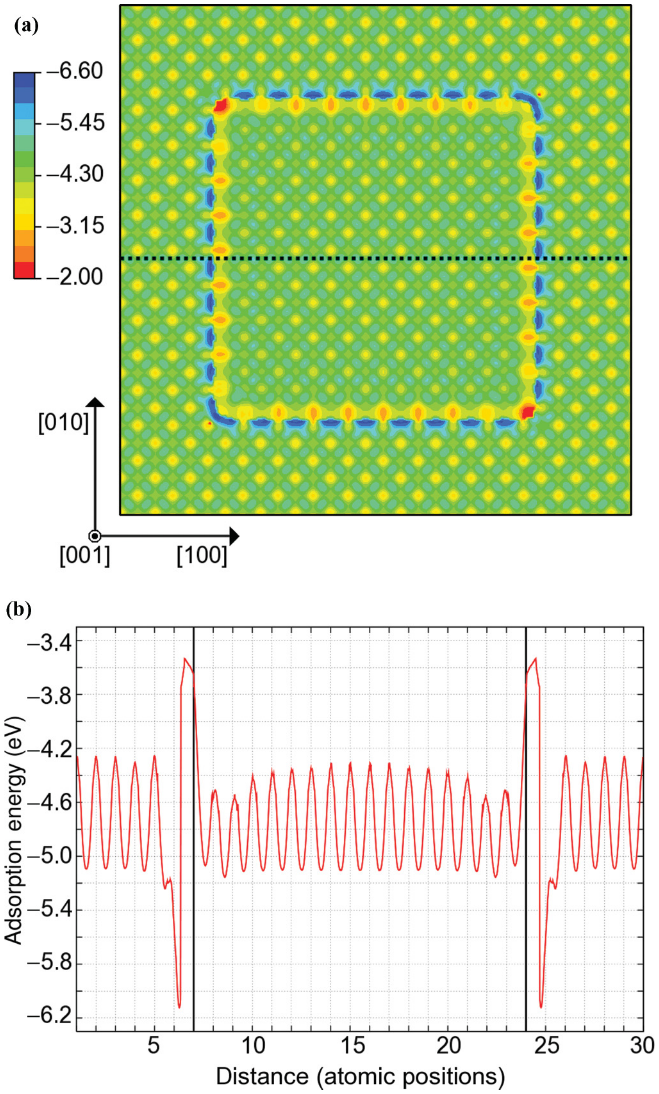

FIG. 1. (Color online) (a) Ti adatom adsorption energy landscape, obtained from static MD calculations, across a one-atom high TiN island on TiN(001). The color scale is expressed in electron volts. (b) Ti adatom adsorption energy line profile from the island center over the island edge and onto the terrace along the preferential in-plane [100] diffusion channel indicated with a dashed line in (a).

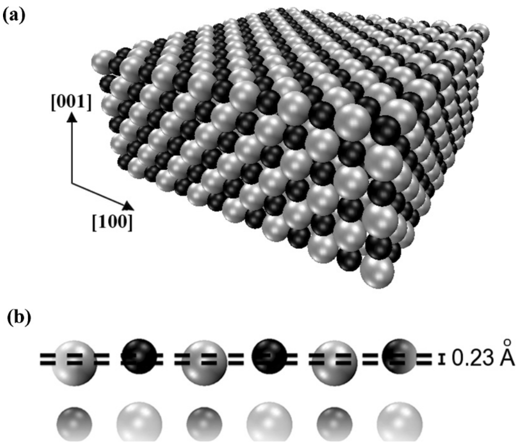

FIG. 2. (a) TiN(001) substrate slab for TiN(001) surface dynamics simulations. N atoms are black; Ti atoms are gray. (b) Magnified image showing surface relaxation.

for N and Ti adatoms in our independent MD runs. There is also a local adsorption energy minimum for N adatoms atop Ti terrace atoms, with $E_{\text{ad}} = -1.5$ eV. Adsorption energies for N are much smaller than the binding energy of constituent N atoms in a N_2 gas-phase molecule (-4.88 eV), indicating that N is considerably more stable in the gas phase than as a free, adsorbed adatom on TiN(001).

In order to observe the behavior of N_2 molecules on TiN(001), two N atoms are placed on the surface, one at a bulk site and the other, in separate runs, along the [110] direction at distances ranging from 0.6 to 4.6 Å. For each calculation, the N atoms are fixed in x and y and can relax in z, while terrace atoms can relax in all directions. The N_2 binding energy—the difference between the energy of the system (two N atoms plus the relaxed substrate) and the energy of the relaxed substrate plus the sum of the N atom adsorption energies—is then determined vs separation d. The results show that for $d > 2.5$ Å, the two adatoms do not interact; with d between ∼1.3 and 2.5 Å, the interaction is repulsive with a barrier of ∼1.7 eV; and with $d < 1.3$ Å there is an attractive interaction. Ten additional tests were carried out at 300 K in which the two N atoms were placed 1.3 Å apart and their motion followed. On each occasion, as expected, N_2 molecules form and desorb at kinetic rates.

Single Ti adatoms are observed, in all cases, to migrate among energetically favored fourfold hollow surfaces sites. The primary diffusion mechanism is that of single jumps along [100] and [010] directions. Out of a total of 2082 migration events recorded, Ti adatoms move via single jumps 1958 times (∼94% of all events). As illustrated in Fig. 3(a), each single diffusion jump contributes d_{NN} to the total Ti migration distance. Diffusion via double jumps, 105 events along in-plane ⟨100⟩ directions, is observed in ∼5% of all cases. Each Ti adatom double jump contributes $2d_{\text{NN}}$ per translation event [Fig. 3(b)]. Longer jumps are not observed. The least-frequent diffusion event is that of diagonal jumps between fourfold hollow sites, corresponding to migration of $\sqrt{2}d_{\text{NN}}$ along the [110] direction, through a metastable

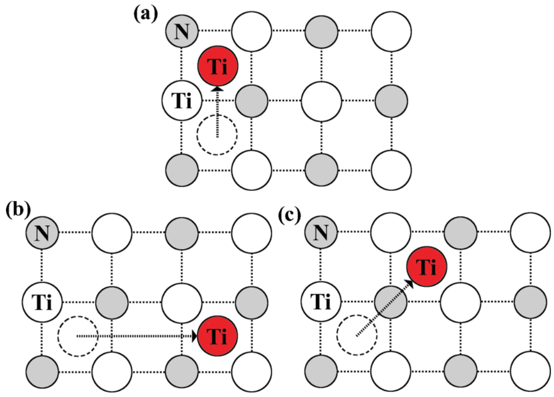

FIG. 3. (Color online) Schematic illustration of Ti adatom diffusion paths on TiN(001). (a) Single jump along the [010] channel, (b) double jump along the [100] channel, and (c) [110] diffusion across an atop N terrace atom position.

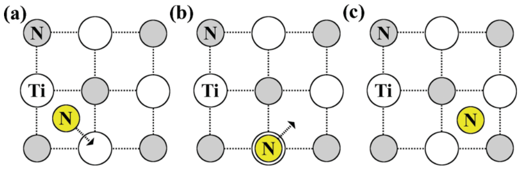

FIG. 4. (Color online) Schematic illustration of N adatom diffusion paths on TiN(001). (a) N originates in its most stable position at a fourfold hollow site and moves along [$1\bar{1}0$] to one of the nearest-neighbor bulk positions atop a Ti terrace atom. (b) The N adatom diffuses to a nearest-neighbor fourfold hollow site to regain its most stable adsorption position. (c) Final N adatom position.

position over the N terrace atom, as illustrated in Fig. 3(c). This diffusion pathway is observed on only 19 occasions (1% of all diffusion events recorded). Overall, the total Ti adatom migration distance $d_{\text{tot}} = d_{\text{net}}$ during 0.25 μs is $2195 d_{\text{NN}}$, corresponding to a velocity $v_{\text{tot}} = v_{\text{net}}$ of 18.6 Å/ns. The surface diffusion coefficient D and prefactor D_0 for Ti adatoms are 0.52×10^{-6} and 5.6×10^{-3} cm^2/s, respectively.

N adatoms are found to reside close to fourfold hollow terrace sites more than 99% of the time. However, their diffusion pathway is quite different than that of Ti adatoms. As illustrated in Fig. 4, migration between neighboring fourfold hollow sites always proceeds along $\langle 110 \rangle$ during which N adatoms pass through metastable positions on top of Ti terrace atoms. The migration distance per event is $\sqrt{2} d_{\text{NN}}$. Consistent with the considerably higher N adatom diffusion barrier, compared with Ti adatoms (see Table III), N diffusion events are much less frequent. We record, for the same 0.25-μs total simulation time, 938 diffusion events and a total migration distance $d_{\text{tot}} = 1327 d_{\text{NN}}$, yielding a migration velocity $v_{\text{tot}} = 11.3$ Å/ns.

In contrast to Ti adatoms, many N migration events involve jumps from metastable positions back to the initial sites, which do not contribute to net diffusion. The number of net migration events recorded is 695, with a net migration distance $d_{\text{net}} = 791 d_{\text{NN}}$, and corresponding velocity $v_{\text{net}} = 6.7$ Å/ns. The lower mobility of N vs Ti adatoms results in a N surface diffusion coefficient value, $D = 0.26 \times 10^{-6}$ cm^2/s, which is half of that obtained for Ti adatoms. Inserting D and the N adatom diffusion barrier E_S of 1.1 eV (Table III) into Eq. (3) yields a prefactor $D_0 = 9.1 \times 10^{-2}$ cm^2/s. Overall, these results eloquently demonstrate the anisotropy of N vs Ti adatom transport on TiN(001). The preferred diffusion channels for Ti adatoms are along in-plane $\langle 100 \rangle$ directions, whereas N adatoms only diffuse along in-plane $\langle 110 \rangle$ directions.

For TiN dimer migration, we choose the initial Ti and N positions to be their bulk sites in the [001] stacking sequence; Ti atoms are placed on top of N terrace atoms and N atoms atop nearest-neighbor Ti terrace atoms. TiN dimers are never observed to dissociate or desorb. The most stable dimer configuration corresponds to the Ti atom residing at a fourfold hollow site with the N atom at a nearest-neighbor bulk position atop Ti, as shown in Fig. 5(a).

TiN dimers migrate on the TiN(001) surface via three different pathways. The most frequently observed diffusion pathway is dimer rotation, which consists of a 90° rotation of the dimer axis with respect to a vertex located at the N dimer atom site. As shown in Fig. 5, the process entails the migration of the Ti dimer atom from its initial hollow site to a neighboring hollow site, in a circular motion via a bulk site atop the N terrace atom, while the N dimer atom remains anchored at its bulk site. This process, which corresponds to a dimer GC migration of $d_{\text{NN}}/\sqrt{2}$, is observed on 572 occasions, or ~58% of the total diffusion events recorded; 312 of these are net diffusion events accounting for 43% of the net dimer diffusion distance. Double rotation events, i.e., two rotation events in succession leading to a 180° rotation of the dimer axis, are observed 11 times. Thus, diffusion via rotation yields a total dimer migration distance of $420 d_{\text{NN}}$, with $v_{\text{tot}} = 3.6$ Å/ns. The corresponding net values are $d_{\text{net}} = 164 d_{\text{NN}}$ and $v_{\text{net}} = 1.4$ Å/ns.

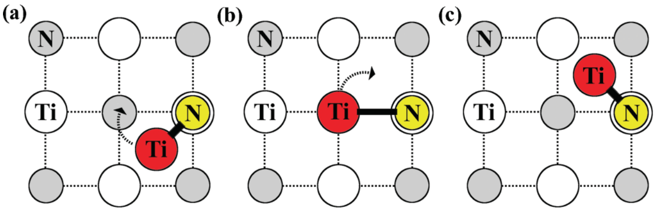

FIG. 5. (Color online) Schematic illustration of TiN dimer diffusion via rotation on TiN(001). (a) The TiN dimer in its most stable adsorption position rotates 45° such that the Ti atom moves from a fourfold hollow site to a bulk site, while the N atom remains anchored in its bulk position. (b) The TiN dimer rotates an additional 45° from bulk epitaxial sites such that the Ti adatom moves to an adjacent fourfold hollow site. (c) Final TiN dimer position.

The second diffusion mechanism observed for TiN dimers is translation via concerted migration of Ti and N atoms along an in-plane $\langle 110 \rangle$ direction. In this process, the two dimer atoms move simultaneously: Ti between neighboring hollow sites, passing over the N terrace atom, and the N dimer atom between neighboring bulk sites on top of Ti terrace atoms, passing through a hollow site, as illustrated in Fig. 6. Dimer diffusion in this manner yields a net GC migration distance of $\sqrt{2} d_{\text{NN}}$ and is observed to occur 241 times, ~25% of the total number of dimer diffusion events, and accounts for 33% of all net diffusion events. Dimer $\langle 110 \rangle$ translation always yields net migration and contributes $341 d_{\text{NN}}$ to the total migration distance with a velocity $v_{\text{tot}} = v_{\text{net}} = 0.89$ Å/ns.

The third dimer diffusion mechanism involves rototranslation, a combination of dimer axis rotation and concerted dimer

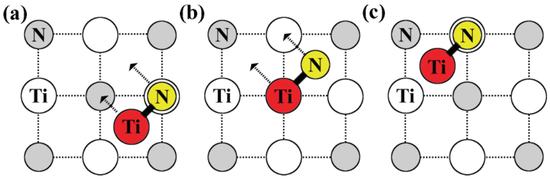

FIG. 6. (Color online) Schematic illustration of TiN dimer diffusion via translation on TiN(001). (a) The dimer atoms translate concertedly along an in-plane [110] channel such that the N adatom moves from its epitaxial position to a fourfold hollow, while the Ti adatom moves to its bulk site. (b) The concerted diagonal motion of dimer atoms continues along the [110] direction, such that the N adatom moves to a nearest-neighbor bulk position and the Ti adatom occupies a fourfold hollow site. (c) Final TiN dimer position.

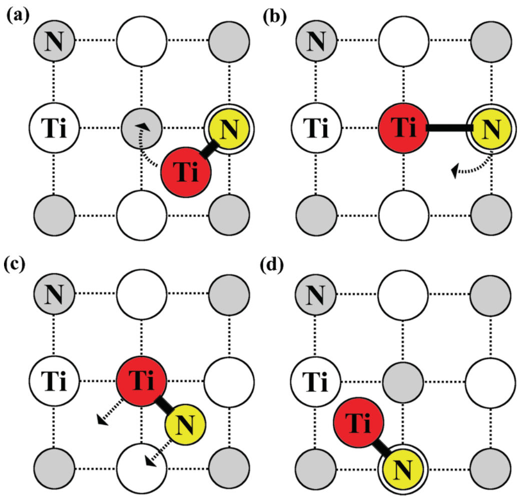

FIG. 7. (Color online) Schematic illustration of TiN dimer diffusion via rototranslation on TiN(001). (a) The TiN dimer in its most stable adsorption position rotates 45° such that the Ti atom moves from a fourfold hollow site to a bulk site, while the N atom remains anchored in its bulk position. (b) The TiN dimer rotates an additional 45° from bulk epitaxial sites such that the N adatom moves to an adjacent fourfold hollow site. (c) The dimer adatoms translate concertedly along an in-plane [110] channel. (d) Final TiN dimer position.

translation. The rototranslation sequence is initiated with a dimer rotation in which the Ti adatom moves from a fourfold hollow site to the N atop site [Fig. 7(a)] with the N dimer atom anchored. In this position, the Ti-N dimer bond length is stretched from $\sqrt{2}d_{NN}/2$ to d_{NN}. The N adatom then rotates from a Ti atop site to the vacated fourfold hollow site [Fig. 7(b)] with Ti remaining stationary. The rototranslation migration sequence is completed with a concerted dimer translation along a $\langle 110 \rangle$ direction such that the two constituent atoms regain their stable positions [Figs. 7(c) and 7(d)]. Rototranslation is observed on 159 occasions, or more then 16% of the total number of dimer diffusion events and 22% of net diffusion events. Each dimer rototranslation event corresponds to a total GC migration distance of $\sqrt{2}d_{NN}$. The total migration distance for dimer diffusion via rototranslations is $225d_{NN}$, and the net migration is $178d_{NN}$, with corresponding velocities $v_{tot} = 1.91$ and $v_{net} = 1.51$ Å/ns.

The aggregate number of dimer diffusion events is 983, with $d_{tot} = 986d_{NN}$ and $v_{tot} = 8.4$ Å/ns. The corresponding overall net values are 723 events, $d_{net} = 682d_{NN}$, and $v_{net} = 5.8$ Å/ns. These results clearly show that TiN dimers are much less mobile, as expected, than both Ti and N adatoms on TiN(001). Thus, the TiN dimer diffusion barrier is larger than that of Ti ($E_s = 0.8$ eV) and N adatoms ($E_s = 1.1$ eV). This conclusion is supported by both DFT calculations[11] and experimental VT-STM results.[4–6] We obtain a surface diffusion coefficient $D = 0.21 \times 10^{-6}$ cm^2/s for TiN dimers; the diffusion barrier E_s is >1.1 eV for this admolecule (Table III); thus, the corresponding prefactor is $>7.6 \times 10^{-2}$ cm^2/s.

The same approach used for TiN dimers is adopted for selecting the starting configurations for TiN_2 trimers in each MD run; individual atoms are placed at bulk positions. The two Ti-N trimer bonds are at right angles with bond lengths of d_{NN}. This is the most stable configuration for TiN_2 trimers based upon DFT calculations at $T_s = 0$ K.[11] However, in each of the 25 independent MD runs, the right-angle bonding configuration transforms into a linear molecule within the first 0.1 ps. The most stable configuration for TiN_2 trimers observed in our 1000-K simulations is shown in Fig. 8(a): Ti is in a fourfold hollow site with the two opposed N atoms in bulk atop positions along $\langle 110 \rangle$ directions. Ti-N bond-lengths in this configuration are $\sqrt{2}d_{NN}/2$.

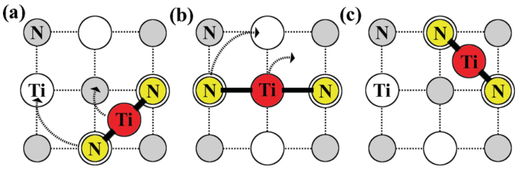

FIG. 8. (Color online) Schematic illustration of TiN_2 trimer diffusion via rotation on TiN(001). (a) The TiN dimer in its most stable adsorption position rotates clockwise 45° with one N atom anchored at its epitaxial site, such that all trimer atoms move to bulk sites. (b) The TiN_2 trimer rotates an additional 45° clockwise such that the most stable configuration is regained. (c) Final TiN_2 trimer position.

Diffusion mechanisms observed for TiN_2 trimers are similar to those discussed above for TiN dimers, rotation, and translation, except that rototranslation is not observed. Trimer rotation, as shown in Fig. 8, involves a 90° concerted rotation of N and Ti around the second N atom, which is anchored. Thus, the trimer molecule remains linear as the bonds are stretched to d_{NN} midway through the rotation, at which point all three trimer atoms briefly occupy bulk sites [Fig. 8(b)] before completing the rotation event and regaining the most stable trimer position [Fig. 8(c)]. The total GC migration distance is $\sqrt{2}d_{NN}$, twice that for TiN dimer rotation. As illustrated in Fig. 9, trimer translation involves concerted diagonal $\langle 110 \rangle$ migration of all three trimer atoms with the admolecule remaining linear. The net trimer GC migration distance d_{net} is $\sqrt{2}d_{NN}$. During translation, the two trimer bonds retain their stable lengths throughout the diffusion event.

Surprisingly, TiN_2 trimers exhibit significantly higher mobility than TiN dimers. During 0.25 μs of simulation time, we record a total of 1196 trimer diffusion events for a total migration distance $d_{tot} = 1691d_{NN}$ with a migration velocity $v_{tot} = 14.3$ Å/ns. Net diffusion corresponds to 915 events, with $d_{net} = 1060d_{NN}$ and $v_{net} = 9.0$ Å/ns. Thus, TiN_2 trimers exhibit surface mobilities which are almost twice

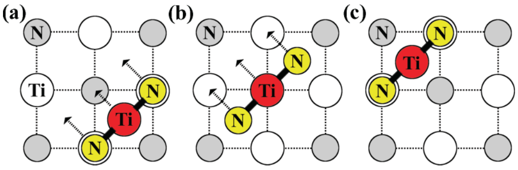

FIG. 9. (Color online) Schematic illustration of TiN_2 trimer diffusion via translation on TiN(001). (a) The trimer atoms translate concertedly along an in-plane [110] channel such that the N adatoms move from their epitaxial positions into adjacent fourfold hollow sites and the Ti adatom moves to its bulk site. (b) The concerted diagonal motion of trimer atoms continues along the [110] direction, such that the most stable trimer configuration is regained. (c) Final TiN_2 trimer position.

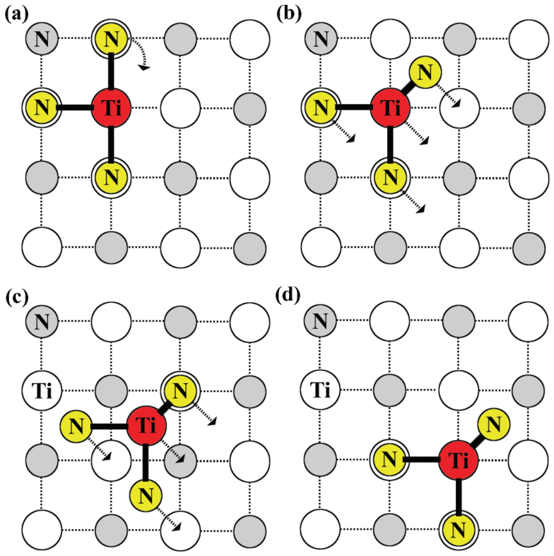

FIG. 10. (Color online) Schematic illustration of TiN$_3$ tetramer diffusion via rotation and translation on TiN(001). (a) Initial TiN$_3$ T-shape configuration with all adatoms in their bulk sites; one of the two N adatoms forming the top of the T moves to an adjacent fourfold hollow site. (b) TiN$_3$ tetramer concerted translation along the [110] channel such that tetramer adatoms in bulk sites move to adjacent fourfold hollow sites and the N adatom in the fourfold hollow site moves to a bulk site. (c) The concerted translation of tetramer adatoms continues along the [110] direction such that the Y configuration again occupies its more stable position, with the Ti adatom in a bulk site. (d) Final TiN$_3$ tetramer position.

that of TiN dimers. The trimer surface diffusion coefficient is $D = 0.28 \times 10^{-6}$ cm^2/s. Using the calculated range for trimer diffusion barriers E_s (Table III) yields a prefactor value D_0 ranging from 3.0×10^{-3} to 9.7×10^{-2} cm^2/s. Trimer diffusion is observed to occur primarily via rotation, which accounts for 94% of the 1126 diffusion events. Rotation leading to net diffusion is observed on 845 occasions and 92% of all net diffusion events. Concerted trimer translation occurs in only 70 occasions and 6% of total trimer diffusion events. Every trimer translation event leads to net diffusion. Thus, translation accounts for 8% of trimer net diffusion events.

The initial TiN$_3$ tetramer configuration used in our simulations, in which each of the four tetramer atoms are at their bulk sites in the [001] stacking sequence and the three N-Ti bonds form two 90° angles and one 180° angle in a T shape, is shown in Fig. 10(a). The Ti tetramer atom resides on bulk sites atop the N terrace atom for most of the total simulation time. In contrast, one of the three N tetramer atoms frequently initiates tetramer rotation events by moving from bulk to fourfold hollow sites, while the other tetramer atoms remain anchored at bulk sites, as illustrated in Fig. 10(a). Thus, the shape of the admolecule changes from a T [Fig. 10(a)] to a Y configuration [Fig. 10(b)]. The three Ti-N bonds now form two ~135° angles and a 90° angle. From this position, the T configuration is regained as the rotated N tetramer atom either moves back to its initial bulk site or forward to a new bulk site. Only the two N tetramer atoms forming the Ti-N bonds along the top of the T configuration can initiate a rotation event in this fashion; the N atom at the base of the T is firmly anchored at its bulk site. This leads to an almost continuous rotation of the admolecule. More than 3×10^5 T–Y–T rotation events are observed, with approximately equal residence times in T and Y configurations. However, such rotations do not lead to tetramer GC migration.

In spite of the continuous rotation described above, TiN$_3$ tetramers, which are expected to be present in significant concentrations during TiN(001) growth at higher N$_2$/Ti flux ratios,[11,27] are found to have very low mobilities on TiN(001). We observe a total of only four GC motions, each a translation yielding net diffusion along in-plane $\langle 110 \rangle$ directions, during the entire 0.25 μs. Tetramer translation is only initiated with the admolecule in a Y configuration as in Fig. 10(b). All tetramer atoms then move in a concerted fashion along an in-plane $\langle 110 \rangle$ direction, such that the Y configuration, with approximately constant average N-Ti bond angles and lengths, is maintained. The Ti atom moves diagonally from a bulk to a metastable fourfold hollow site, the two N atoms representing the arms of the Y move from bulk to hollow sites, and the N atom representing the base of the Y moves from a hollow to a bulk site above a Ti terrace atom [Fig. 10(c)]. The migration event is completed as the tetramer atoms regain their stable positions [Fig. 10(d)]. Each translation event yields a net GC migration distance of $\sqrt{2}d_{\mathrm{NN}}$. Overall, this corresponds to a total migration distance $d_{\mathrm{tot}} = d_{\mathrm{net}} = 5.7d_{\mathrm{NN}}$ and a migration velocity $v_{\mathrm{tot}} = v_{\mathrm{net}}$ of only 0.05 Å/ns. The low tetramer mobility results in a correspondingly low-surface diffusion coefficient, $D = 0.13 \times 10^{-8}$ cm^2/s with a prefactor, accounting for a diffusion barrier $E_s \gg 1.1$ eV, of $D_0 \gg 4.5 \times 10^{-4}$ cm^2/s.

IV. DISCUSSION

The diffusion mechanisms, total and net migration distances during 0.25 μs, and migration velocities for Ti and N adatoms and TiN$_x$ (x = 1–3) admolecules, on TiN(001), are summarized in Table IV, while calculated surface diffusion coefficients D and prefactors D_0 are listed in Table V. Our results demonstrate that Ti adatoms have the highest mobilities; they diffuse primarily via single jumps of length d_{NN} along [100] and [010] directions. However, long jumps of $2d_{\mathrm{NN}}$ in these directions are also observed and account for ~10% of the total migration distance. We note that self-diffusion via double jumps has been observed experimentally for single metal adatoms on low-index metallic surfaces[50,51] and In long jumps on InGaAs(001) are predicted by DFT calculations.[52] Ti adatom migration along $\langle 110 \rangle$ directions is the least-frequent event observed, accounting for just 1% of the total migration distance. Ti atoms are the only adspecies for which each migration event, irrespective of the migration pathway, is a translation leading to net GC diffusion on TiN(001).

The strong anisotropy in the migration of Ti adatoms is surprising in view of the relatively small difference, obtained from static calculations, in energy barriers along $\langle 100 \rangle$ and $\langle 110 \rangle$ directions, 0.8 eV and 0.9 eV, respectively. We ascribe the directional anisotropy to $\langle 110 \rangle$ steric hindrance provided by N terrace atoms with an average relaxed lattice position 0.12 Å above the median (001) terrace plane, combined with

TABLE IV. Summary of results for Ti, N, and TiN_x admolecule ($x = 1$–3) diffusion on TiN(001).

		Total diffusion			Net diffusion		
Diffusing species	Mechanism	Number of events	Migration d_{tot} (d_{NN})	Velocity v_{tot} (Å/ns)	Number of events	Migration d_{net} (d_{NN})	Velocity v_{net} (Å/ns)
Ti adatom		2082	2195	18.62	2082	2195	18.62
	Single	1958(94%)	1958(89%)		1958(94%)	1958(89%)	
	Double	105(5%)	210(10%)		105(5%)	210(10%)	
	Diagonal	19(1%)	27(1%)		19(1%)	27(1%)	
N adatom		938	1327	11.26	695	791	6.71
	Translation	938(100%)	1327(100%)		695(100%)	791(100%)	
TiN dimer		983	986	8.37	723	682	5.79
	Rotation	572(58%)	404(41%)		312(43%)	156(23%)	
	Translation	241(25%)	341(34%)		241(33%)	341(50%)	
	Rototranslation	159(16%)	225(23%)		159(22%)	178(26%)	
	Double-rotation	11(1%)	16(2%)		11(2%)	8(1%)	
TiN_2 trimer		1196	1691	14.35	915	1060	8.99
	Rotation	1126(94%)	1592(94%)		845(92%)	961(91%)	
	Translation	70(6%)	99(6%)		70(8%)	99(9%)	
TiN_3 tetramer		$>3 \times 10^5$	6	0.05	4	6	0.05
	Rotation	$>3 \times 10^5$ ($\sim$100%)	0(0%)		0(0%)	0(0%)	
	Translation	4 ($\sim$0%)	6(100%)		4(100%)	6(100%)	

a relatively large vibrational amplitude, 0.13 Å, due to the low N atomic mass.

N adatoms are considerably less mobile than Ti adatoms. Single N adatoms, which reside at fourfold hollow sites for essentially the entire simulation time, diffuse only diagonally, along ⟨110⟩ directions, through a metastable position atop a neighboring Ti terrace atom. From this site, N moves forward to a new hollow site or back to the initial hollow site with equal probability. Thus, N adatoms exhibit much lower ($\sim$60%) total migration distances and velocities than Ti atoms (Table IV) and a surface diffusion coefficient, which is half that obtained for Ti adatoms (Table V). The net velocity of N adatoms, further reduced due to the frequent forward/back motion, is only 36% that of Ti adatoms.

As expected, TiN_x adspecies on TiN(001) exhibit lower mobilities and more complex surface diffusion pathways than adatoms. The most frequent migration event observed for TiN_x admolecules is rotation, which accounts for 58% of all TiN dimer events and 94% of TiN_2 trimer events. TiN_3 tetramers exhibit almost continuous rotation; none of which leads to net GC migration. The other migration mechanism observed for all three admolecules is translation, which leads in all instances to net GC migration. For TiN dimers, we also observe rototranslation, a combination of rotation and translation. Overall, TiN dimers are found to have $\sim$86% of the net mobility of N adatoms and $\sim$32% of the mobility of Ti adatoms. This is also reflected in their relative surface diffusion coefficients (see Table V). In contrast, TiN_3 tetramers are essentially stationary on TiN(001), with only four concerted translation events observed in 0.25 μs. TiN_3 mobilities are two orders of magnitude lower than those of both Ti and N adatoms. Thus, tetramers, residing on epitaxial sites, lead directly to local island growth on TiN(001).

TABLE V. Calculated surface diffusion coefficients D and prefactors D_0 for each adspecies.

Diffusing species	Surface diffusion coefficient D (cm^2/s)	Prefactor D_0 (cm^2/s)[a]
Ti adatom	0.52×10^{-6}	5.6×10^{-3}
N adatom	0.26×10^{-6}	9.1×10^{-2}
TiN dimer	0.21×10^{-6}	$>7.6 \times 10^{-2}$
TiN_2 trimer	0.28×10^{-6}	3.0×10^{-3}–9.7×10^{-2}
TiN_3 tetramer	0.13×10^{-8}	$\gg 4.5 \times 10^{-4}$

[a] Determined using the diffusion activation energies in Table III.

Cluster motion primarily occurs through a combination of translation and rotation events. The general trend in the results for TiN_x clusters on TiN(001) is that as x is increased from 1 to 3, each additional N atom facilitates the occurrence of rotation events, while reducing the number of translation events: 572 rotation and 241 translation events for TiN dimers; 1126 rotation and 70 translation events for TiN_2 trimers; and $>3 \times 10^5$ rotation events, with only four translation events, for TiN_3 tetramers (Table IV). The opposing trends lead to significantly increased GC mobility for TiN_2. However, this is not the case for TiN_3 tetramers, which primarily only rotate in place with essentially no net translation. Initiating tetramer translation requires all four atoms comprising the admolecule to simultaneously vibrate in the same direction.

Surprisingly, TiN_2 trimers have considerably higher net velocities than TiN dimers and even N adatoms. Indeed, TiN_2 mobilities, controlled primarily by GC motion via rotation events, are almost half that of Ti adatoms. The same trend is observed in terms of surface diffusion coefficients values (Table V). The significantly increased mobility of trimers vs

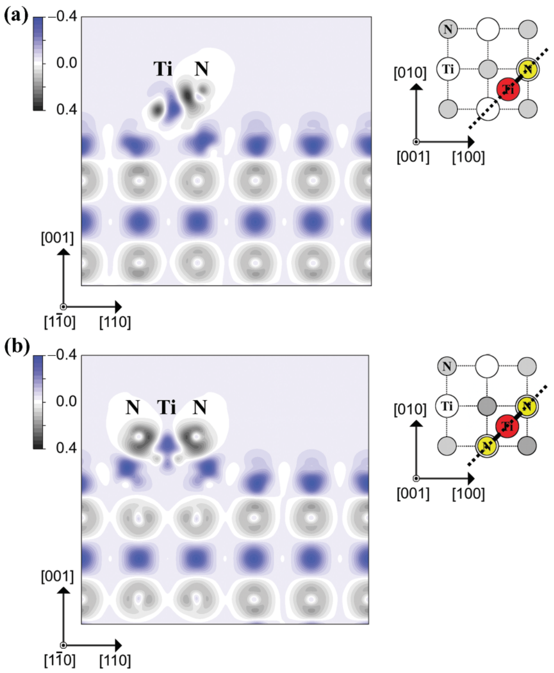

FIG. 11. (Color online) Charge transfer maps for (a) a TiN dimer and (b) a TiN$_2$ trimer absorbed at their most stable positions on TiN(001) and plotted along the directions shown by the corresponding inserts. Color scale is expressed in electrons per angstrom cubed.

dimers and tetramers is not due to size-dependent compact vs noncompact shape differences as proposed for small Rh clusters on Rh(001).[53] To explain the TiN$_2$ behavior, we carry out DFT calculations, using the same VASP parameters described in Sec. II, to probe TiN$_x$/terrace-atom interactions in the most stable configuration for each cluster size. For this purpose, larger atomic slabs, containing 3 × 3 unit cells in each layer for a total of 180 atoms, and 3 × 3 × 1 k-point grids, are employed.

DFT cluster results are presented in Fig. 11 as maps of net charge transfer between terrace atoms and in-plane intracluster bonds. That is, the maps plot color-coded differences between the charge density distributions in gas phase N and Ti atoms and the atoms in the chemisorbed relaxed TiN$_x$/TiN(001) systems. In each panel, blue (medium gray) represents decreased electron density, black denotes increased electron density, and white corresponds to regions with no charge transfer. As expected, Ti cluster cations, in all cases, donate negative charge to intracluster N anions. The amount of intracluster charge transfer and, importantly, the charge exchange with terrace atoms is significantly different for the three TiN$_x$ admolecules.

For TiN addimers [Fig. 11(a)], the net charge transfer yields a more strongly ionic in-plane Ti-N bond. As a result of the dimer charge distribution asymmetry, both Ti and N dimer atoms interact strongly with neighboring Ti terrace atoms. That is, Ti terrace atoms donate electron charge to Ti dimer atoms. This is denoted in Fig. 11(a) by the black lobe between the Ti adatom and the nearest-neighbor Ti terrace atom. The N dimer atom is strongly bonded in its bulk position atop a Ti terrace atom that also donates electron charge to the N adatom. The combination of the strong Ti-dimer/Ti-terrace bond and the N being anchored in an epitaxial position explains the low rotational frequency of TiN admolecules (Table IV).

In contrast, the in-plane Ti-N bonds of TiN$_2$ trimers have a much more highly symmetric charge distribution as shown in Fig. 11(b). The two N trimer atoms are in bulk sites, strongly interacting with Ti terrace atoms underneath. The N adatoms receive electron charge density from the Ti trimer atom as well as the nearest-neighbor Ti terrace atoms. However, in this case there is no strong interaction between the Ti trimer atom and neighboring Ti terrace atoms. Thus, either of the N trimer atoms can act as rotational anchor site as the opposite N trimer

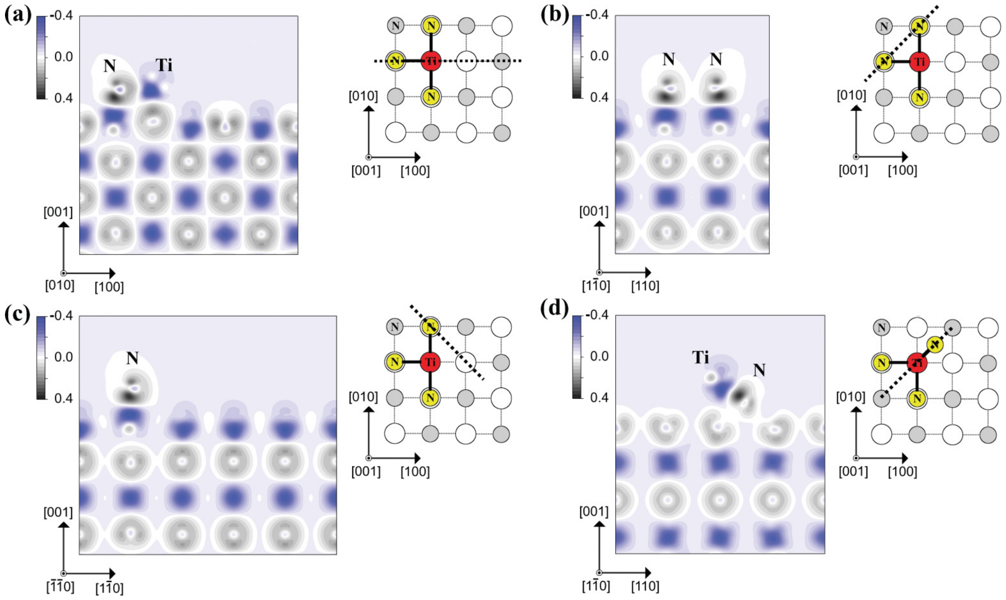

FIG. 12. (Color online) Charge transfer maps for a TiN$_3$ tetramer absorbed on TiN(001): (a)–(c) charge density differences for the tetramer in a T configuration plotted along the directions shown by the inserts; (d) charge density difference for the tetramer in a Y configuration plotted along the direction shown in the insert. Color scale is expressed in electrons per angstrom cubed.

atom initiates rotation. Consequently, the trimer rotational probability is significantly higher than that for dimers. At 1000 K, adatoms and terrace atoms vibrate at high frequencies, and the N trimer atom with an instantaneously weaker bond to Ti terrace atoms is the one that originates the rotation event.

Figure 12 shows DFT charge transfer maps for the TiN_3 tetramers plotted in several directions. Charge distribution is locally symmetric along both the [100] and [110] directions for the T configuration [Figs. 12(a) and 12(b)]. The Ti adatom is anchored through strong interactions with terrace atoms and the N tetramer atom forming the base of the T [Fig. 12(a)], which, due to electronic repulsion cannot rotate toward the N adatoms forming the top of the T [see Fig. 12(b)]. However, the charge distribution plot along the $[1\bar{1}0]$ direction [Fig. 12(c)] demonstrates that the two upper N adatoms of the T are free to rotate and change the tetramer configuration from T to Y, leaving the rotated N adatom in a hollow site [Fig. 12(d)]. From this position, the N adatom can easily move back or forward to more stable bulk sites atop Ti terrace atoms. This process leads to essentially continuous tetramer rotation with no net GC motion.

V. CONCLUSIONS

Investigations of the dynamics of atomic-scale transport processes on TiN(001) reveal several key features in the migration kinetics of Ti, N, and TiN_x complexes with $x = 1$–3. Ti adatoms have a significantly lower diffusion activation energy than N adatoms. At 1000 K, they migrate with velocities almost three times that of N adatoms. The primary diffusion mechanism for Ti adatoms is that of single nearest-neighbor distance jumps among fourfold hollow sites along in-plane $\langle 100 \rangle$ channels. Longer jumps occur at much lower frequency. By contrast, N adatoms exhibit much lower migration rates than Ti and diffuse only along in-plane $\langle 110 \rangle$ directions. TiN_x complexes, as expected, have lower mobilities than both Ti and N adatoms and diffuse via complex migration pathways involving rotation, translation, and rototranslation. As x increases from 1 to 3, the probability for TiN_x admolecule translation events decreases, while the probability for rotations increases significantly. The opposing trends give rise to TiN_2 trimers exhibiting surprisingly high mobilities, higher than for N adatoms and nearly half that of Ti adatoms. TiN_3 tetramers, however, are essentially stationary, with mobilities more than two orders of magnitude lower than Ti and N adatoms. Thus, tetramers, residing on epitaxial sites, lead directly to island growth on TiN(001).

ACKNOWLEDGMENTS

We received financial support from the Swedish Research Council (VR) for the Linköping Linnaeus Initiative LiLi-NFM on Nanoscale Functional Materials (Grant No. 2008-6572) and the Swedish Government Strategic Research Area Grant in Materials Science (No. Mat-LiU 2009-00971) on Advanced Functional Materials. We acknowledge P. Münger for useful discussions and P. Steneteg for support in video editing. Calculations were performed using the resources provided by the Swedish National Infrastructure for Computing (SNIC) and on the Neolith and Kappa Clusters located at the National Supercomputer Centre (NSC) in Linköping.

---

[*] Corresponding author: davsan@ifm.liu.se

[1] See discussion in review article, S. Kodambaka, S. V. Khare, I. Petrov, and J. E. Greene, Surf. Sci. Rep. **60**, 55 (2006), and references therein.

[2] T. Paskova, V. Darakchieva, P. P. Paskov, J. Birch, E. Valcheva, P. O. A. Persson, B. Arnaudov, S. Tungasmita, and B. Monemar, Phys. Status Solidi C **2**, 2027 (2005).

[3] M. H. Xie, S. M. Seutter, W. K. Zhu, L. X. Zheng, H. S. Wu, and S. Y. Tong, Phys. Rev. Lett. **82**, 2749 (1999).

[4] S. Kodambaka, V. Petrova, A. Vailionis, P. Desjardins, D. G. Cahill, I. Petrov, and J. E. Greene, Surf. Rev. Lett. **7**, 589 (2000).

[5] S. Kodambaka, V. Petrova, A. Vailionis, P. Desjardins, D. G. Cahill, I. Petrov, and J. E. Greene, Thin Solid Films **392**, 164 (2001).

[6] S. Kodambaka, V. Petrova, A. Vailionis, I. Petrov, and J. E. Greene, Surf. Sci. **526**, 85 (2003).

[7] F. Watanabe, S. Kodambaka, W. Swiech, J. E. Greene, and D. G. Cahill, Surf. Sci. **572**, 425 (2004).

[8] S. Kodambaka, N. Israeli, J. Bareno, W. Swiech, K. Ohmori, I. Petrov, and J. E. Greene, Surf. Sci. **560**, 53 (2004).

[9] J. Bareno, S. Kodambaka, S. V. Khare, W. Swiech, V. Petrova, I. Petrov, and J. E. Greene, Advanced Summer School in Physics, AIP Conf. Proc. **885**, 205 (2007).

[10] M. A. Wall, D. G. Cahill, I. Petrov, D. Gall, and J. E. Greene, Phys. Rev. B **70**, 035413 (2004).

[11] D. Gall, S. Kodambaka, M. A. Wall, I. Petrov, and J. E. Greene, J. Appl. Phys. **93**, 9086 (2003).

[12] B. Alling, P. Steneteg, C. Tholander, F. Tasnadi, I. Petrov, J. E. Greene, and L. Hultman, Phys. Rev. B **85**, 245422 (2012).

[13] H. Ljungcrantz, M. Oden, L. Hultman, J. E. Greene, and J. E. Sundgren, J. Appl. Phys. **80**, 6725 (1996).

[14] J. E. Sundgren, Thin Solid Films **128**, 21 (1985).

[15] J. E. Greene, J. E. Sundgren, L. Hultman, I. Petrov, and D. B. Bergstrom, Appl. Phys. Lett. **67**, 2928 (1995).

[16] C. S. Shin, S. Rudenja, D. Gall, N. Hellgren, T. Y. Lee, I. Petrov, and J. E. Greene, J. Appl. Phys. **95**, 356 (2004).

[17] P. Hedenqvist, M. Bromark, M. Olsson, S. Hogmark, and E. Bergmann, Surf. Coat. Technol. **63**, 115 (1994).

[18] T. Polcar, T. Kubart, R. Novak, L. Kopecky, and P. Siroky, Surf. Coat. Technol. **193**, 192 (2005).

[19] A. S. Ingason, F. Magnus, J. S. Agustsson, S. Olafsson, and J. T. Gudmundsson, Thin Solid Films **517**, 6731 (2009).

[20] D. McIntyre, J. E. Greene, G. Hakansson, J. E. Sundgren, and W. D. Munz, J. Appl. Phys. **67**, 1542 (1990).

[21] L. A. Donohue, I. J. Smith, W. D. Munz, I. Petrov, and J. E. Greene, Surf. Coat. Technol. **94-95**, 226 (1997).

[22] D. Gall, I. Petrov, and J. E. Greene, J. Appl. Phys. **89**, 401 (2001).

[23] H. S. Seo, T. Y. Lee, I. Petrov, J. E. Greene, and D. Gall, J. Appl. Phys. **97**, 083521 (2005).

[24] C. S. Shin, D. Gall, Y. W. Kim, P. Desjardins, I. Petrov, J. E. Greene, M. Oden, and L. Hultman, J. Appl. Phys. **90**, 2879 (2001).

[25] S. Veprek, M. G. J. Veprek-Heijman, P. Karvankova, and J. Prochazka, Thin Solid Films **476**, 1 (2005).

[26] L. Hultman, *Synthesis, Structure, and Properties of Super-Hard Superlattice Coatings* (Plenum Press, London, 2006).

[27] M. A. Wall, D. G. Cahill, I. Petrov, D. Gall, and J. E. Greene, Surf. Sci. **581**, L122 (2005).

[28] F. H. Baumann, D. L. Chopp, T. D. de la Rubia, G. H. Gilmer, J. E. Greene, H. Huang, S. Kodambaka, P. O'Sullivan, and I. Petrov, MRS Bull. **26**, 182 (2001).

[29] S. Kodambaka, S. V. Khare, V. Petrova, A. Vailionis, I. Petrov, and J. E. Greene, Surf. Sci. **513**, 468 (2002).

[30] U. Helmersson, J. E. Sundgren, and J. E. Greene, J. Vac. Sci. Technol. A **4**, 500 (1986).

[31] B. W. Karr, I. Petrov, P. Desjardins, D. G. Cahill, and J. E. Greene, Surf. Coat. Technol. **94-95**, 403 (1997).

[32] S. Plimpton, J. Comput. Phys. **117**, 1 (1995).

[33] B. J. Lee and M. I. Baskes, Phys. Rev. B **62**, 8564 (2000).

[34] Y. M. Kim and B. J. Lee, Acta Mater. **56**, 3481 (2008).

[35] G. Kresse and J. Hafner, Phys. Rev. B **47**, 558 (1993).

[36] J. P. Perdew and Y. Wang, Phys. Rev. B **45**, 13244 (1992).

[37] P. E. Blöchl, Phys. Rev. B **50**, 17953 (1994).

[38] L. E. Toth, *Transition Metal Carbides and Nitrides* (Academic Press, New York, 1971).

[39] T. Lee, K. Ohmori, C. S. Shin, D. G. Cahill, I. Petrov, and J. E. Greene, Phys. Rev. B **71**, 144106 (2005).

[40] J. O. Kim, J. D. Achenbach, P. B. Mirkarimi, M. Shinn, and S. A. Barnett, J. Appl. Phys. **72**, 1805 (1992).

[41] V. A. Gubanov, A. L. Ivanovsky, and V. P. Zhukov, *Electronic Structure of Refractory Carbides and Nitrides* (Cambridge University Press, Cambridge, 1994).

[42] L. Hultman, J. E. Sundgren, and J. E. Greene, J. Appl. Phys. **66**, 536 (1989).

[43] D. G. Sangiovanni, V. Chirita, and L. Hultman, Phys. Rev. B **81**, 104107 (2010).

[44] M. Marlo and V. Milman, Phys. Rev. B **62**, 2899 (2000).

[45] C. V. Ciobanu, D. T. Tambe, and V. B. Shenoy, Surf. Sci. **582**, 145 (2005).

[46] M. P. Allen and D. J. Tildesley, *Computer Simulation of Liquids* (Oxford University Press, Oxford, 1989).

[47] L. Hultman, S. A. Barnett, J. E. Sundgren, and J. E. Greene, J. Cryst. Growth **92**, 639 (1988).

[48] E. P. Munger, V. Chirita, J. E. Sundgren, and J. E. Greene, Thin Solid Films **318**, 57 (1998).

[49] D. Adamovic, E. P. Munger, V. Chirita, L. Hultman, and J. E. Greene, Appl. Phys. Lett. **86**, 211915 (2005).

[50] T. R. Linderoth, S. Horch, E. Laegsgaard, I. Stensgaard, and F. Besenbacher, Phys. Rev. Lett. **78**, 4978 (1997).

[51] G. Antczak and G. Ehrlich, Phys. Rev. Lett. **92**, 166105 (2004).

[52] E. Penev, S. Stojkovic, P. Kratzer, and M. Scheffler, Phys. Rev. B **69**, 115335 (2004).

[53] G. L. Kellogg, Prog. Surf. Sci. **53**, 217 (1996).